International Journal of Mechanical Sciences 243 (2023) 108048

Contents lists available at ScienceDirect

International Journal of Mechanical Sciences

journal homepage: www.elsevier.com/locate/ijmecsci

Modelling of a shear-type piezoelectric actuator for AFM-based vibration-assisted nanomachining

Bo Xue [a,b], Emmanuel Brousseau [a,*], Chris Bowen [c]

[a] Cardiff School of Engineering, Cardiff University, Cardiff, United Kingdom
[b] College of Mechanical and Electrical Engineering, Northeast Forestry University, Harbin, China
[c] Department of Mechanical Engineering, University of Bath, Bath, United Kingdom

ARTICLE INFO

Keywords:
AFM-based vibration-assisted nanomachining
Coupled field FE modelling

ABSTRACT

Recent research investigations have reported the benefit of enhancing conventional AFM-based nanoscale machining operations by the introduction of high frequency vibrations between the AFM tip and the processed material. The technique relies on piezoelectric actuation and is relatively straight forward to implement in practice. However, the non-linearity of piezoelectric actuators when operated under high electric field and frequency conditions can affect the dimensional accuracy of the fabricated nanostructures. To address these issues, the paper reports a method based on coupled mechanical-electrical Finite Element (FE) modelling to predict the relative motion between an AFM tip and a workpiece for vibration-assisted AFM-based nanomachining applications. In particular, the novelty of the proposed method is that it combines two classical approaches for modelling the nonlinear behaviour of piezoelectric materials. More specifically, two sources of nonlinearity are considered simultaneously by combining the field-dependant model from Muller and Zhang with the frequency-dependant model from Damjanovic. The resulting combined model is employed to establish the piezoelectric constitutive equations implemented in the developed coupled field FE model. A further distinguishing characteristic of the work is that the proposed approach was subsequently validated by comparing the predicted widths of nanoscale grooves against those machined with a custom AFM-based vibration-assisted nanomachining configuration.

1. Introduction

Nanostructures can provide improved performances and advanced functionalities in modern devices [1,2]. To support the manufacturing requirements of such structures, nanofabrication technologies, e.g. nanolithography [3], additive nanomanufacturing [4], laser nanomanufacturing [5] and nanomechanical machining [6], have attracted sustained attention from the research community, and have developed rapidly as a result. Based on the fact that nanomechanical machining enables the processing of a wide range of materials and exhibits high processing flexibility, this fabrication technique is of important interest in this context. Amongst the different possible implementations of the cutting process, vibration-assisted machining (VAM) has also been proposed for fabricating micro and nanostructures [7–9]. In such configurations, the auxiliary cutting motion normally employed to improve cutting conditions in conventional VAM could be utilised directly for the generation of nanostructures.

Nanoscale AFM-based VAM is an emerging research area aligned with such efforts. Indeed, a number of recent studies have proposed enhancing standard AFM tip-based nanomachining operations by introducing vibratory motions between the tip of the AFM probe and the workpiece [10]. Research investigations have highlighted the positive effects of implementing the AFM-based nanomachining process in a vibration-assisted mode. For example, Park and co-workers [11] found that AFM-based VAM reduced the cutting forces and burr formation, while Zhang and co-workers [12] and Geng and co-workers [13] reported that this could lead to a reduction in tip wear. In such studies, piezoelectric-based actuation configurations are used to drive the workpiece, or the tip itself. Specific solutions have relied on flexure-based [14] or flexure-inspired [15] designs to increase the amplitude of motions generated by longitudinal piezoelectric stacks. Other AFM-based VAM studies have reported on customised actuation designs, for which either the AFM probe [16] or the workpiece [17] has been mounted directly on the piezoelectric actuator. Such flexure-less

* Corresponding author.
E-mail address: BrousseauE@cardiff.ac.uk (E. Brousseau).

https://doi.org/10.1016/j.ijmecsci.2022.108048
Received 16 September 2022; Received in revised form 10 December 2022; Accepted 15 December 2022
Available online 20 December 2022

designs typically allow for the utilisation of a more flexible operating range for the vibratory driving signal as they are not restricted to the resonance frequency of the flexure device. In addition, such customised piezoelectric solutions often operate in open-loop mode for implementing AFM-based VAM. This can lead to improved processing speed since it avoids restrictions associated with the limited frequency bandwidth of control systems. However, this also leads to undesirable phenomena associated with piezoelectric materials such as hysteresis and creep, which can decrease the accuracy and predictability of displacements of such piezoelectric based designs [18,19]. In addition, unlike the auxiliary nature of piezoelectric actuation observed in conventional VAM [14], the actual sub-μm motion generated by such actuators for nanomachining applications has a direct influence on the dimensional accuracy of the resulting nanostructures formed. In particular, out-of-plane AFM-based VAM and in-plane AFM-based VAM configurations influence the depth and the width, respectively, of machined grooves. The amplitude of vibratory motions can also influence the process mechanics, such as the size of the undeformed chip thickness [20,21]. Therefore, it is important to characterise and predict the dynamic behaviour of such open-loop piezoelectric-based solutions to develop robust AFM tip-based vibration-assisted nanomachining platforms.

Based on the principle of the direct and converse piezoelectric effects, energy harvesters [22,23] and micro/nanometre actuators [24,25] are the two main applications of piezoelectric materials. Due to the polarization direction perpendicular to the electric field direction, shear mode piezoelectricity can provide bending deformation [26] and shear deformation [27]. Though the piezoelectric coefficient of shear mode (d_{15}) is generally larger than that of the transverse mode (d_{31}) and longitudinal mode (d_{33}) and thus, results in larger deformations under an identical electric field intensity, it is often not exploited due to its deformation configuration [23,25]. However, shear-type piezoelectric actuation shows advantages in the context of AFM-based VAM. This is because 1D or 2D machining trajectories with a relatively large amplitude range can be directly generated by the shear deformation of piezoelectric stacks without complex ancillary set-up. In addition, revolving trajectories with radii larger than one hundred nanometres can be generated, leading to the implementation AFM-based nanomilling operations [28]. This specific process development was reported to be beneficial for the fabrication of complex nanostructures with changeable dimensions and for improving the processing efficiency and quality [29,30]. However, the nonlinearity of piezoelectric materials still affects the dimensional accuracy of generated structures in this case.

In this context, the focus of the research reported here is to present, implement and validate a methodology for predicting the dynamic response of the combined "tip-workpiece-actuator" system for a customised AFM-based VAM set-up under a range of driving frequencies and voltages. In particular, we present a coupled mechanical-electrical finite element (FE) model to describe theoretically the motions of a shear-type piezoelectric actuation set-up for 1D and 2D in-plane AFM-based VAM when the workpiece is directly mounted on the actuator. AFM-based VAM experiments are also performed on a single crystal copper workpiece to verify the robustness of the proposed methodology. The distinguishing characteristic of this research is that the nonlinearity of piezoelectric actuator displacements is considered and modelled as a function of both the electric field *and* the frequency of the driving signal. More specifically, this is achieved by combining two classical models from the field of piezoelectric ceramic materials. The remaining parts of this paper are organised as follows. The next section presents the experimental procedures implemented and the novel methodology adopted to develop a numerical model of the AFM-based VAM set-up developed in this research. In the subsequent section, simulation results are presented and compared with actual AFM-based nanomachining experiments. Finally, conclusions and outlook for future work are reported.

2. Methodology: experimental procedures and numerical modelling

2.1. Piezoelectric actuation solution for AFM-based VAM

A two-dimensional shear-type piezoelectric stack (model NAC2902-H2.8 from Noliac, Denmark) was employed in this study. Fig. 1 shows an annotated image of this actuator. The piezoelectric element was composed of a stack of two shear actuator plates (model CSAP02 from Noliac, Denmark) which were orientated in such a way to have their respective polarisation directions and shear strain directions perpendicular to each other; i.e. along the x-axis and y-axis, respectively, according to the coordinate system shown in Fig. 1. Each plate was made of a soft piezoceramic material referred to as NCE51 by the manufacturer, while their nominal dimensions was 5 mm × 5 mm × 0.5 mm and their nominal maximum shear displacement was 1.5 μm under a drive voltage of 320 V. Each such shear-type element was sandwiched between two isolation plates. These isolation layers were made of unpolarised piezoceramic material while the electrodes were in stainless steel. The two end isolation plates (c.f. Fig. 1) were customised to have a thickness of 1 mm to ease clamping during the experiments.

2.2. Piezoelectric constitutive equations: proposed approach for modelling nonlinear effects

To develop a mechanical-electrical coupled field model, the following piezoelectric constitutive equations must be implemented:

$$\begin{cases} S = s.T + d^t.E \\ D = d.T + \varepsilon.E \end{cases} \tag{1}$$

where S is the strain, T is the stress (N m^{-2}), D is the electric charge density displacement (C m^{-2}) and E is the strength of the electric field (V m^{-1}). In addition, the material properties in these equations are d, the piezoelectric coefficients (m V^{-1}), ε, the permittivity coefficients (F m^{-1}) and s, the elastic compliance coefficients (Pa^{-1}). The constitutive equations bridge the link between the mechanical and electrical loads. For example, as a result of the direct piezoelectric effect, an applied mechanical stress, T, produces the electrical displacement, D, in the piezoelectric material; while the application of an electric field,E, leads to a mechanical strain, S, of the piezoelectric material as a result of the converse piezoelectric effect. In the case of a shear mode actuator, the electric field is applied perpendicular to the polarisation so that shear piezoelectric coefficients (e.g. d_{15}) are important.

It should be noted that most FE-based simulation models use constant piezoelectric coefficients when implementing the above constitutive equations [31–35]. However, when the external electric field exceeds a threshold value, piezoelectric coefficients can no longer be considered constant due to the motions of non-180° domain walls of the ferroelectric materials [36–39]. This is especially the case for the shear coefficient of interest in this research, i.e. d_{15}, which governs the in-plane displacement of shear-type piezoelectric materials [40,41]. As a result, piezoelectric actuator set-ups operated in open loop may be reasonably predictable when driven under low electric field conditions due to limited domain motion [42]. However, when the actuator is subjected to high electric fields to achieve a high motion amplitude, the nonlinear behaviour of a piezoelectric material must be considered when modelling the system [43–45]. A possible approach to achieve this is through fitting experimental data to the empirical model, as proposed by Mueller and Zhang [40], which expresses the piezoelectric coefficients as field-dependant functions. The use of such nonlinear coefficients into piezoelectric constitutive equations has proven effective for modelling and predicting the nonlinearity of piezoelectric materials [41,46,47]. For this reason, the model from Mueller and Zhang [40] is also considered in this research to implement the developed coupled field FE model. This means that the dependence of the coefficient d_{15} on

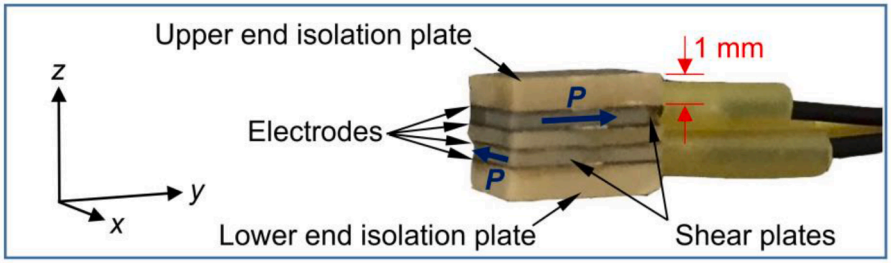

Fig. 1. Annotated photograph of the shear-type piezoelectric stack actuator utilised. The symbol "*P*" and the associated arrows represent the polarisation direction for each active plate.

the electric field, E_1, orientated perpendicular to the polarisation direction is given as follows:

$$d_{15}(E_1) = d_{\text{lin}}[1 + (d_{\text{nl}}E_1)^{\alpha}] \tag{2}$$

where d_{lin} is the low-field piezoelectric constant, d_{nl} is the nonlinear coefficient of piezoelectric constant and α is usually assumed to be equal to 1.2.

In addition, Masys et al. [48] investigated the effect of the applied drive frequency on the response of the piezoelectric coefficient d_{15}. The results reported by these authors showed that the dynamic behaviour of the piezoelectric material is affected by nonlinearity in this case as well. This is due to the higher frequency of operation resulting in fewer domains being able to keep pace with the rapidly changing electric field. In turn, this leads to a decrease of d_{15} with frequency [48]. To take this additional source of nonlinearity into consideration in this research, we propose to integrate the work of Damjanovic [49] into the model of Mueller and Zhang [40]. In particular, Damjanovic observed that the value of the piezoelectric coefficient d_{33} decreases linearly with the logarithm of the frequency. This is due to the frequency dependence of the domain-wall mobility as reported by Garcia [38]. For this reason, in this research, it is proposed that the model of Damjanovic [49] is combined into the model of Mueller and Zhang [40] by expressing the d_{lin} and d_{nl} coefficients from Eq. (2) as logarithmic function of the frequency, as follows:

$$d_{\text{lin}}(f) = a_1 \lg(f) + b_1 \tag{3}$$

$$d_{\text{nl}}(f) = a_2 \lg(f) + b_2 \tag{4}$$

where f is the applied frequency and where a_1, b_1, a_2, and b_2 are constants which are determined experimentally. As a result, the following expression is proposed for d_{15}:

$$d_{15}(E_1, f) = d_{\text{lin}}(f)[1 + (d_{\text{nl}}(f)E_1)^{\alpha}] \tag{5}$$

where $d_{\text{lin}}(f)$ and $d_{\text{nl}}(f)$ are not considered constants, as would be the case when implementing the model from Mueller and Zhang [40], and we define these coefficients according to Eqs. (3) and (4), respectively. In practice, the above expression is employed as the objective function to be fitted with experimental data. These data are obtained by characterising the actuator displacements for a range of electric field and frequency values. Next, once the necessary constants a_1, b_1, a_2, and b_2 have been identified, the resulting expression for $d_{15}(E_1,f)$ is fed into the developed coupled field FE model for simulating the dynamic displacement of each shear-type piezoelectric plate that composes the NAC2902-H2.8 actuator used in this study.

2.3. Coupled field FE model

A FE-based modelling approach is used to take into account the coupled field effect described earlier to predict the dynamic response of piezoelectric materials, in particular for set-ups exhibiting relatively complex geometrical configurations and boundary conditions. In this work, a FE model was developed with the software Abaqus based on a Lagrangian formulation. Fig. 2 depicts the complete model of the "tip-workpiece-actuator" system developed for AFM-based VAM and for which the nonlinear displacement behaviour was accounted for via the expression proposed with Eq. (5) for $d_{15}(E_1,f)$. Fig. 2(a) presents a schematic of the experimental set-up, in which the cutting forces (F_x, F_y, F_z) induced by the AFM probe tip were applied as load boundary conditions in the FE simulation. Fig. 2(b) shows the developed FE model. Fig. 2(c) is the exploded view of the FE model for the shear piezoelectric stack. As can be seen in this figure, the model consisted of three isolation end plates, four pieces of stainless steel electrodes (60 μm thick) and two shear piezoelectric plates bonded together using the "Tie" constraint in Abaqus. The top and bottom end plates were made of the non-polarized NCE51 material and had a thickness of 1 mm, while the middle plate was 0.5 mm thick. A local coordinate system (1–2–3), as shown in Fig. 2(d), was defined to describe the anisotropic properties of ferroelectric materials and the polarisation direction was set along the 3-axis. For a shear-type piezoelectric actuator, when the electric field is applied along the 1-direction, the shear strain of the plate is generated in the 1–3 plane. The system of units for the physical quantities was set to be kg-m-s-°C. Correspondingly, the output units of force, stress and electric potential were N, Pa and V, respectively. A 6-node linear piezoelectric triangular prism element (C3D6E) was used to mesh the piezoelectric shear plate with an average side length of about 104 μm. Finally, Table 1 shows the material parameters as provided by the manufacturer. These were employed in the model for each shear actuator plate, except for the shear coefficient parameter d_{15}, which was determined according to the methodology described above; see Eq. (5). In practice, the linear piezoelectric constitutive equations present inside the software Abaqus could be employed, However, for the coefficient d_{15}, the user subroutine USDFLD in Abaqus was implemented to capture the electric field and frequency dependence.

2.4. Experimental set-up: characterisation of the nonlinear piezoelectric coefficient $d_{15}(E_1,f)$ and AFM-based VAM operations

Commonly, three methods can be employed for assessing piezoelectric coefficients, namely the frequency method, the laser interferometry method and the quasi-static method [50]. For piezoelectric actuator applications, the laser interferometry method is the most appropriate, where piezoelectric coefficients are evaluated by measuring the displacement of the actuator. A one-dimensional laser doppler vibrometer (LDV) (model OFV-303 from Polytec, Germany) was employed to measure in-plane shear displacements of the piezoelectric actuator under different driving sinusoidal signals, with peak-to-peak voltage values ranging from 100 V to 250 V and with frequency values comprised between 2 Hz and 10 kHz. Table 2 shows the specific values considered in these experiments. The LDV instrument had a laser wavelength of 633 nm and a resolution of 32 nm. Fig. 3 illustrates the measurement set-up utilised. The input from the signal generator was amplified with a fixed gain of 50 V/V by a power amplifier (model 2100HF from Trek, USA). An oscilloscope was utilised to collect the

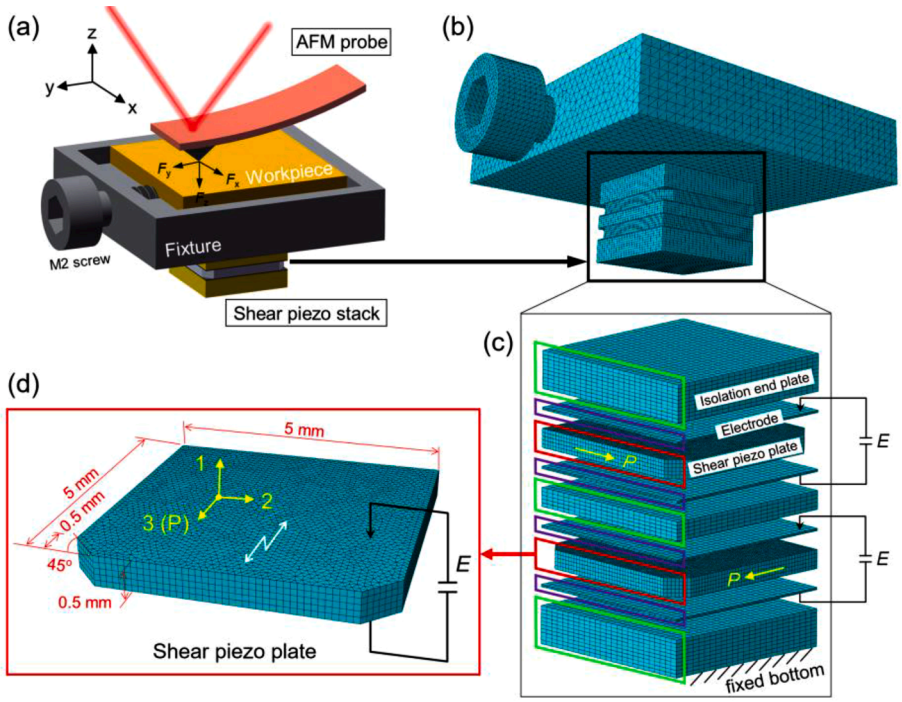

Fig. 2. (a) Schematic AFM-based VAM set-up of the "tip-workpiece-actuator" system, (b) developed FE model, (c) exploded view of the FE model for the shear piezoelectric stack showing the different individual components and (d) single shear piezoelectric plate.

Table 1
Property parameters of the NCE51 material.

Material parameter	Value
Elastic compliance coefficients (10^{-12} m^2/N)	
s_{11}	17.00
s_{12}	−5.36
s_{13}	−8.69
s_{33}	21.30
$s_{44} = s_{55}$	48.90
$s_{66} = 2(s_{11} - s_{12})$	44.72
Permittivity coefficients (10^{-8} F/m)	
$\varepsilon_{11} = \varepsilon_{22}$	1.72
ε_{33}	1.68
Relative permittivity coefficients	
$\varepsilon_{11r} = \varepsilon_{22r}$	1940
ε_{33r}	1900
Piezoelectric coefficients (10^{-12}C/N)	
d_{31}	−208
d_{33}	443
d_{15}	669

Table 2
Experimental conditions used to characterise the actuator displacements.

Driving frequency (Hz)	2, 10, 100, 200, 400, 600, 800, 1000, 2000, 3000, 4000, 5000, 6000, 7000, 8000, 9000,10,000
Driving voltage (V)	+/−50, +/−62.5, +/−75, +/−87.5, +/−100, +/−112.5, +/−125

displacement signals recorded by the LDV. The oscilloscope was also employed to monitor the input from the signal generator to the amplifier for assessing the phase lag between the applied driving signal and the collected displacement signal. This was achieved by comparing the phase spectrums of these two signals at the driven frequency calculated from Fast Fourier Transform (FFT). The measured displacement, u, corresponding to the shear deformation of the piezoelectric actuator, was subsequently used to calculate the shear strain, S, according to the following equation:

$$S = u/t \tag{6}$$

where t is the thickness of the piezoelectric plate. Then, based on the pure converse piezoelectric effect, the piezoelectric coefficient d_{15} could be assessed for each combination of driving voltage and frequency values, as:

$$d_{15} = S/E_1 \tag{7}$$

Furthermore, AFM-based VAM experiments were also conducted to validate the reliability of the proposed modelling method. A simple fixture system was designed that could be fitted on the existing stage of the commercial AFM instrument utilised (model XE-100 from Park Systems, South Korea). The workpiece processed was a single copper crystal specimen with crystallographic planes orientated in the (111) direction and with overall dimensions 10 mm x 10 mm x 0.5 mm. The end isolation plate at the bottom of the piezoelectric actuator was mechanically clamped onto the part of the fixture that was screwed on the AFM stage, while the upper isolation plate was glued on a smaller fixture piece that was designed to hold the copper specimen. The shear-type piezoelectric actuator could be actuated to vibrate along directions of motion within the (xy) plane (c.f. Fig. 2(a)). Nanoscale grooves were machined during a single-pass of the tip along the face-forward direction. Using this set-up, it is possible to conduct 1D and in-plane 2D AFM-based VAM operations. The AFM probe, employed as the cutting tool, was the model DNISP from Bruker (USA). This probe had a nominal spring constant of 225 N/m and was mounted with a diamond cube-corner tip. Finally, the XEL software from Park Systems was utilised to define linear machining trajectories for producing grooves. A constant normal force of 30 μN was maintained between the tip and the workpiece via the feedback loop of the AFM instrument in a similar fashion to contact mode AFM scanning.

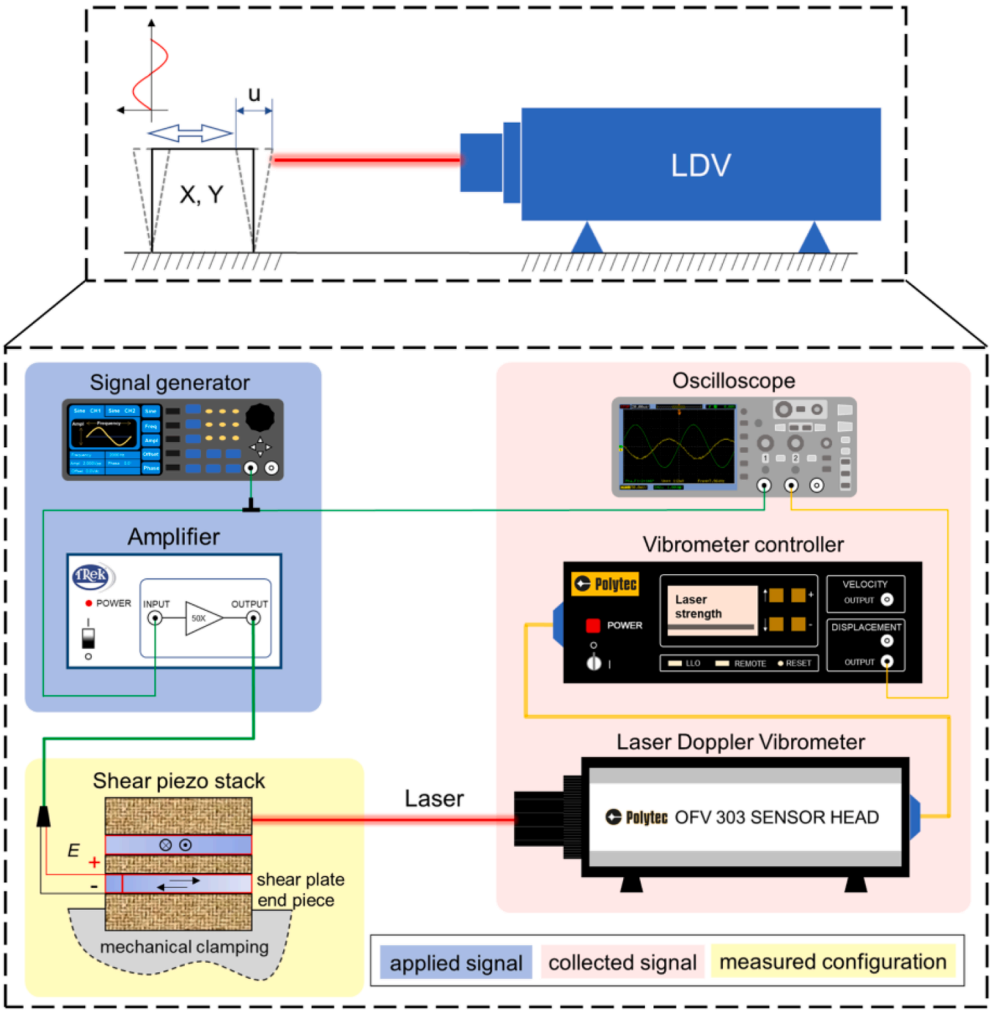

Fig. 3. Schematic of the measurement set-up used to characterise the d_{15} coefficient of the piezoelectric actuator under a range of driving voltage and frequency values.

3. Results and discussion

3.1. Electric field- and frequency-dependant piezoelectric coefficient $d_{15}(E_1,f)$

Fig. 4(a) shows a plot of the displacements recorded using the characterisation set-up depicted earlier in Fig. 3 for a single shear-type piezoelectric plate and considering the entire combination of applied voltage and frequency values provided in Table 2. From this figure, it can be seen that with an increase in frequency, all the displacement amplitudes under the applied voltages first decrease gradually and then increase rapidly once the driving frequency reaches approximately 3 kHz. The *intrinsic* contribution to the total strain is associated with movement of the ionic dipole and is less affected by frequency; however, the *extrinsic* contribution to the total strain as a result of motions of non-180° domain walls at high electric field contributes to greater extent at lower frequencies [36, 51]. It can also be noted that with a higher applied voltage (and associated electric field), the rate of change in the gradual decrease of the displacement amplitude with frequency becomes more pronounced. Again, this is due to domain wall motion acting as an extrinsic contribution to the strain to a greater extent at high electric fields, which needs a finite time to response and hence subsequently reduces with frequency. At relatively low electric fields, domain motion is reduced and the total strain is more dependant on the intrinsic contribution to strain as a result of ion motion, which is less influenced by drive frequency.

Fig. 4(b) presents the displacement of the shear plate and the phase lag between the driving sinusoidal voltage signal and the output displacement signal at different driving frequencies under the applied peak-to-peak voltage of 250 V. In addition, Fig. 4(c) reports three examples of data recorded with the oscilloscope to prepare the graph shown in Fig. 4(b). It can be observed from Fig. 4(b) that a frequency of 3 kHz, where the inflection point for the displacement amplitude was noted, also approximately corresponds to the point at which the phase lag between the input and output signals begins to change sharply, which is not influenced by the electric field. Thus, it can be said that up until 3 kHz, the piezoelectric actuator plate followed a behaviour, which can be described by piezoelectric constitutive equations. The FE analysis revealed that the first order resonance in bending should be around 95 kHz (see the inserted diagram in Fig. 4(b)). Although the maximum driving frequency considered in these characterisation experiments, i.e. 10 kHz, was far away from this first order resonance, with the frequency increasing above 3 kHz, due to the change in phase lag, the actuator entered a region of unstable vibratory behaviour, which could no longer be predicted by piezoelectric constitutive equations. In addition, in this region, the maximum displacement was not generated at the peak of applied sinusoidal voltage as observed with Fig. 4(c). It can be seen in the figure that with increasing frequency the difference of corresponding positions between the peaks of two sinusoidal signals becomes larger. By plotting the displacement against voltage relationship in Fig. 4(c), it was

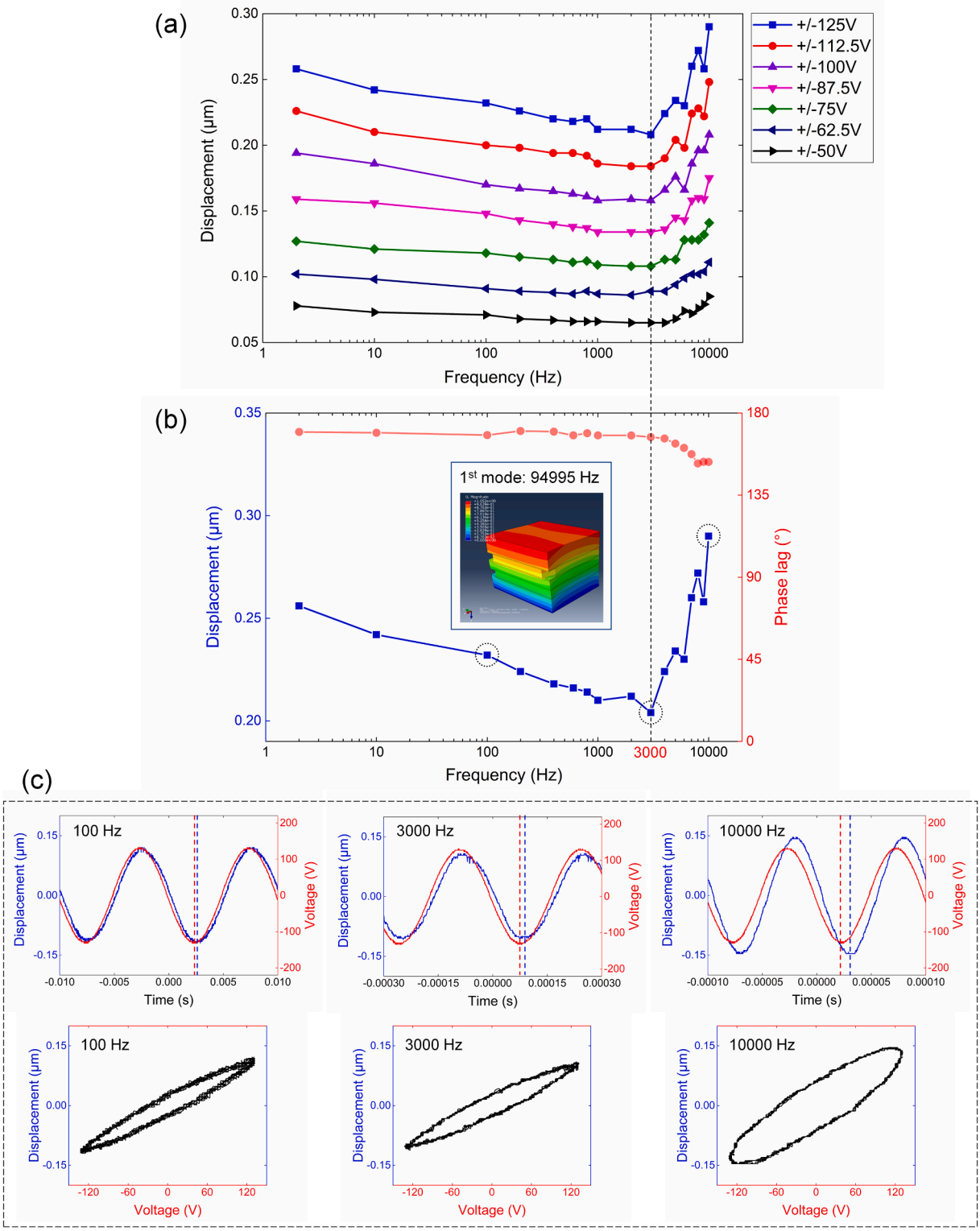

Fig. 4. Experimental data showing (a) the plot of the displacements of the shear piezoelectric plate under different voltage and frequency values, (b) variations of displacement and phase lag versus logarithmic frequency under the voltage of +/−125 V and (c) three examples of typical displacement plots, respectively varying with time and voltage, again under the voltage of +/−125 V.

found that the hysteresis loops of 100 Hz and 3 kHz bear similarities and display sharp reversal peaks at their extrema values, which is characteristic of hysteresis. However, the hysteresis loop for 10 kHz exhibits an elliptical shape with rounded tips, which reflects the behaviour of the piezo stack system rather than the piezoelectric plate only [52]. Hence, it can be concluded that the constant and negligible phase difference before 3 kHz was mainly caused by the hysteresis effect of the piezoelectric ceramic. However, after 3 kHz, the displacement begins to lag behind the excitation voltage and becomes larger. Hence, if the displacement data for frequency values larger than 3 kHz are used to fit the model, the prediction will be inaccurate when the configuration of the piezo stack is changed.

Hence, it was decided that individual experimental data points for the piezoelectric coefficient d_{15} (derived from Eq. (7)) should be obtained only for frequency values in the stable region, i.e. between 2 Hz and 2 kHz. This data collection was also conducted at different applied voltage values and the series of such points then plotted against the electric field, as shown in Fig. 5. In this way, the relationship between d_{15} and E_1 could be calculated based on the power law model from Mueller and Zhang (c.f. Eq. (2)). Fig. 5 shows the fitting obtained for nine different driving frequencies between 2 Hz and 2 kHz. For each case, the power law equation fitted to the data resulted in the identification of a pair of piezoelectric coefficients, i.e. the constant d_{lin} and the nonlinear coefficient d_{nl}. Table 3 presents a summary of the pair of these coefficients obtained for the frequency values considered. In addition, the goodness of fit between the power law model (Eq. (2)) and the original data points was assessed with the traditional R^2 metric. This information is also provided in Table 3. Based on this assessment, given that the best fit resulted in a R^2 value of 99.22% (at 100 Hz) and that the lowest R^2 value was 94.54% (at 10 Hz), it could be stated that the power law from Mueller and Zhang well describes the dynamic response of the shear-type piezoelectric plate for the range of driving frequency signals considered here.

Based on the experimental values for d_{lin} and d_{nl} extracted, as described above for each frequency considered, the next step consisted in fitting these data to the model from Damjanovic [49]. This outcome is shown in Fig. 6 where, based on Eqs. (3) and (4), two expressions could be extracted to characterise the frequency-dependant $d_{\text{lin}}(f)$ and $d_{\text{nl}}(f)$ coefficients. By introducing these two formulas into Eq. (5), a nonlinear function for d_{15}, could be obtained which considered both electric field-dependant and frequency-dependant effects. This expression could be employed in the developed coupled field FE model to predict the dynamic shear response of the NCE51 piezoceramic material for a driving electric field smaller than the coercive field and for a driving frequency less than 2 kHz. It is of interest to note that the reference value of the piezoelectric coefficient, d_{lin}, was given as 669 pC/N by the manufacturer of this piezoactuator (see Table 1), when measured under a very low frequency condition, i.e. 0.2 Hz. By using the frequency dependant expression for d_{lin} extracted in this work, then, under 0.2 Hz, this value was found to be 671.5 pC/N, and thus in good agreement to that given by the manufacturer. This provides a degree of confidence in the approach followed in the study presented here.

Based on the obtained expression for $d_{15}(E_1,f)$, the theoretical displacement of the shear piezoelectric plate could be assessed at higher voltage values as shown in Fig. 7(a). In this figure, the interrupted lines represent the theoretical predicted results for voltage values of +/−200 V, +/−250 V and +/−320 V. In line with recorded experimental data, the model also predicts that the decreasing rate of displacement as the frequency increases is more pronounced at higher voltages. A three-dimensional plot of such variations in displacements in relation to the voltage and frequency is also graphed with Fig. 7(b).

3.2. *Finite element analysis of the electrical and mechanical coupled effect on the piezoelectric trajectory*

By employing the experimentally extracted nonlinear $d_{15}(E_1,f)$

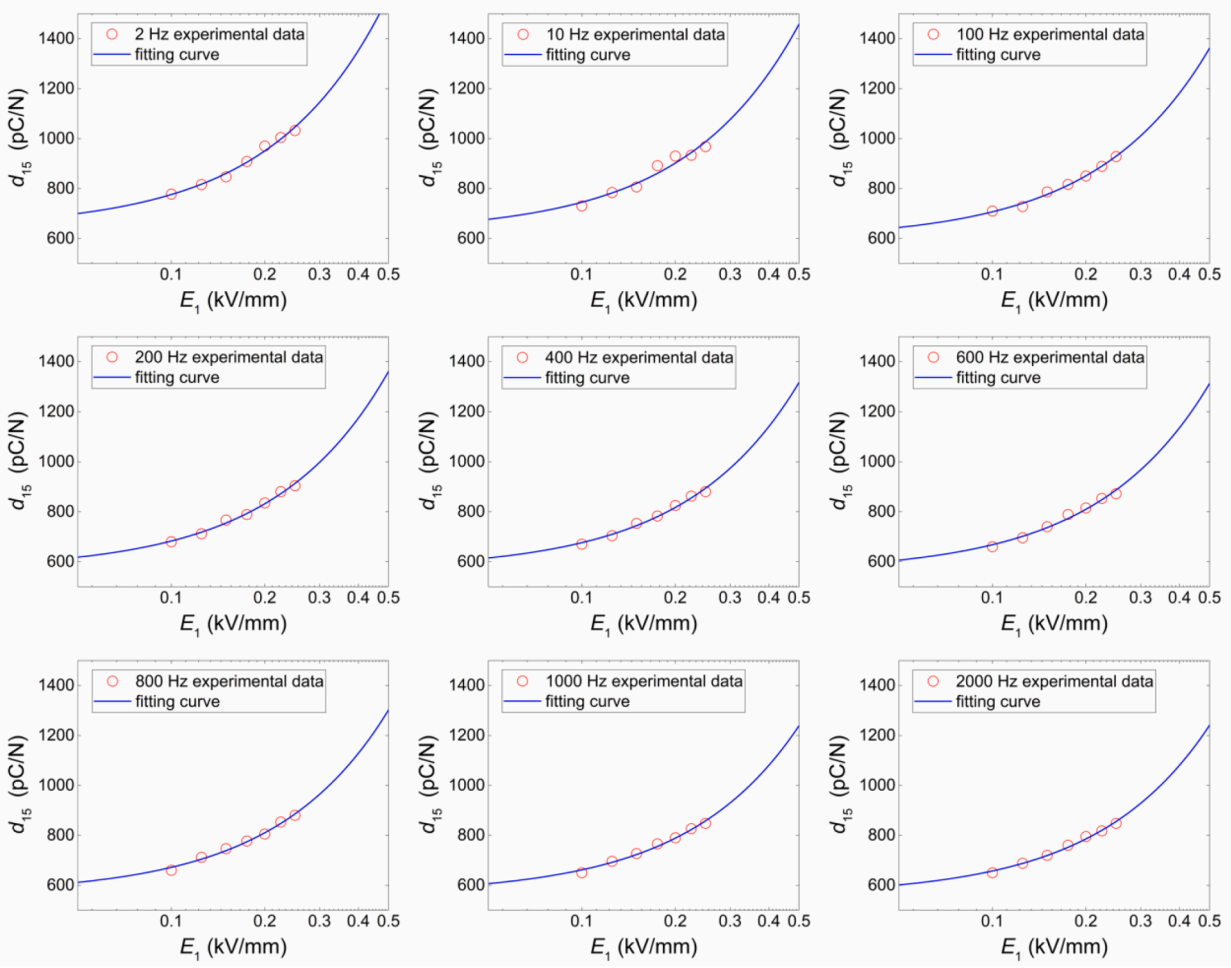

Fig. 5. Experimental data and fitting based on the model from Mueller and Zhang for varying values of d_{15} with E_1 under different frequencies between 2 Hz and 2 000 Hz.

Table 3
Piezoelectric constant d_{lin} and nonlinear coefficient d_{nl} found by fitting the model from Mueller and Zhang [40] to the experimental data for a range of frequency values between 2 Hz and 2 kHz. The R^2 value indicates the goodness of fit.

Frequency (Hz)	2	10	100	200	400	600	800	1000	2000
d_{lin} (pC/N)	641.3	624.4	595.8	568.1	567.9	558.9	565.2	564	558.4
d_{nl} (mm/kV)	2.727	2.546	2.468	2.64	2.519	2.567	2.494	2.324	2.365
R^2(%)	98.6	94.5	99.2	99.1	98.8	98.3	99.0	98.8	99.1

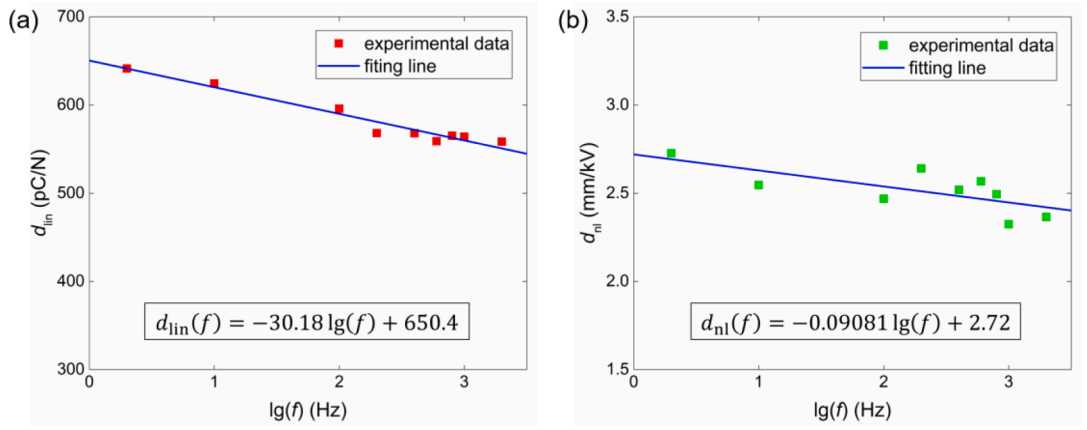

Fig. 6. Experimental data and fitting based on the model from Damjanovic to express (a) the low-field piezoelectric constant $d_{lin}(f)$ and (b) the nonlinear coefficient of piezoelectric constant $d_{nl}(f)$.

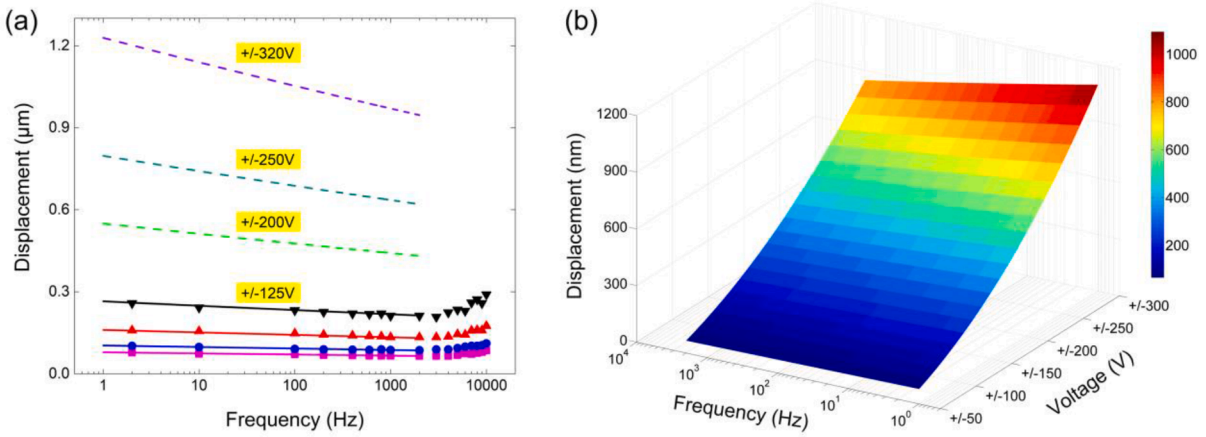

Fig. 7. (a) Displacement of the piezoelectric actuator for peak to peak voltage values in the range 100 V to 640 V and for frequency values from 2 Hz to 2000 Hz. The interrupted lines plot predicted displacements based on the proposed nonlinear $d_{15}(E_1,f)$ function. (b) 3 dimensional plot of such displacement as a function of driving frequency and voltage.

function, FE simulations of the piezoelectric stack under a variety of electrical and mechanical coupled loads were conducted. For 1D vibrations, only one shear plate was actuated using the sinusoidal voltages, while for 2D vibration simulations, two out-of-phase sinusoidal voltages were applied to different shear plates, as illustrated with Fig. 8 (a). Fig. 8(b) and (c) show the simulated displacements of one plate and the resultant trajectories of two plates, respectively, under driving voltage amplitudes of 75 V and 140 V and frequencies of 100 Hz, 500 Hz and 1000 Hz. It can be seen that with varying $d_{15}(E_1,f)$, the displacement of the shear plate is no longer a regular sinusoid. Hence, the revolving trajectories when considering the combined displacement with Fig. 8(c) display a square-like shape, which becomes more obvious under higher voltage condition. It is also noted that a higher frequency has little effect on the resulting shape of the trajectory, but it reduces the amplitude of vibration.

In addition, four types of mechanical traction loads with the same peak value of 10 N were applied to the top surface of the piezoelectric stack, as shown in Fig. 8(d). The condition labelled “d1” is that of a constant force against the moving direction. The condition labelled “d2” aims to represent 1D in-plane VAM. The condition labelled “d3” attempts to model one half of the 2D in-plane VAM, while “d4” aims to represent the whole cycle of 2D in-plane VAM. Fig. 8(e) presents the corresponding simulated displacement results under an electric load of 75 V and frequency of 500 Hz. The objective of these simulations was to assess the influence of the interaction force between the AFM tip and the workpiece surface on the resulting displacement of the piezo electric stack. It can be seen with conditions “d1” and “d2”, that a constant force produces a fixed displacement offset, i.e. about 11 nm for a force of 10 N. Under the conditions “d3” and “d4”, the displacement offset changes constantly with the variation of force. Finally, the displacement under a much lower constant force of 2 mN was also simulated and displayed with the red squares markers in Fig. 8(e). In this case, a negligible

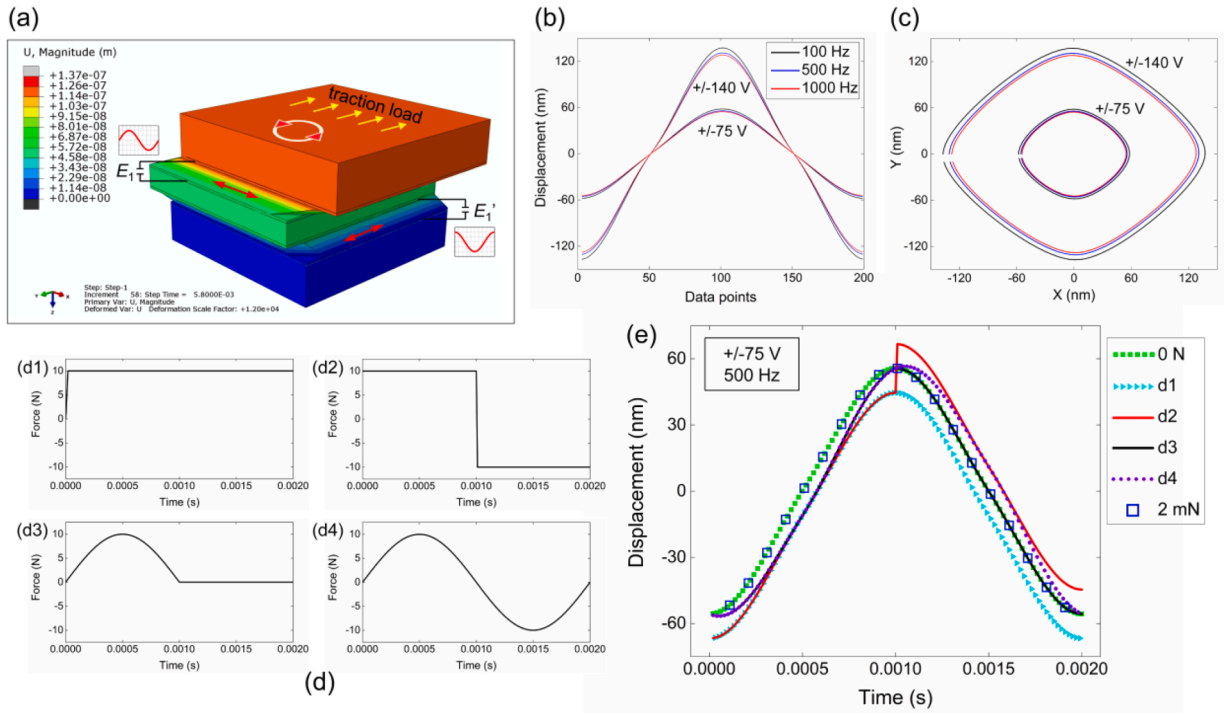

Fig. 8. Motion simulation of the piezoelectric stack under different electrical and mechanical loads. (a) An example of FE outcome displaying displacement contour of the piezoelectric stack, (b) displacements of a single piezoelectric plate at two different driving voltage and three frequency values, (c) resultant displacements from two piezoelectric plates actuated with sinusoidal signals 90° out-of-phase, (d) simulated boundary conditions for the mechanical load and (e) effect of load type on piezoelectric displacement.

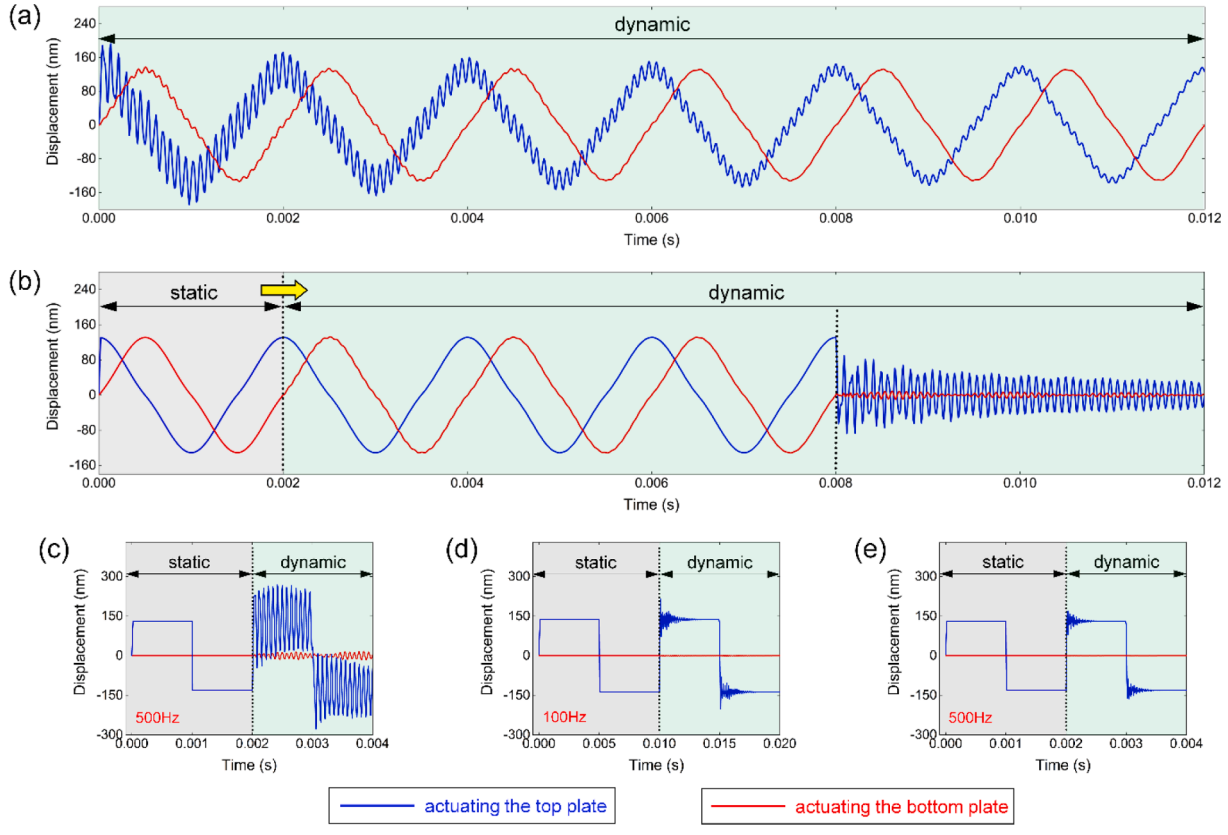

Fig. 9. Dynamic analysis of the VAM set-up and shear piezoelectric stack under different excitation signals for the top and the bottom actuation plates. (a) and (b) dynamic displacement response of the workpiece when driven by out-of-phase sinusoidal signals of +/−140 V at 500 Hz. (c) and (d) dynamic displacement response of the workpiece when driven by a square signal of +/−140 V at 500 Hz and 100 Hz. (e) dynamic displacement response of the top isolation plate without the workpiece and without the fixture when driven by a square signal of +/−140 V at 500 Hz.

displacement offset was predicted. Thus, given that an even lower interaction force of 30 μN was set in this study for the actual AFM-based VAM experiments, it can be said that its influence on the displacements of the shear-type piezoelectric actuator were also negligible. More generally, as the cutting forces in AFM-based nanomachining are commonly less than 1 mN [53,54], their influence on the motions of piezoelectric set-ups similar to that reported in this study could also be neglected.

A dynamic simulation study was also conducted with the developed FE model to analyse the influence of inertial forces on the displacements of the AFM-based VAM set-up (c.f. Fig. 2(a)). Fig. 9(a) displays the simulated dynamic displacements when the top and bottom shear-type piezoelectric plates are driven by a sinusoidal signal of +/−140 V at 500 Hz. Based on this figure, the model indicates that undesired high frequency vibrations are generated when the input voltage increases instantaneously at the beginning of the application of the driving signal. However, these oscillations decrease reasonably rapidly after an elapsed time equal to a few periods of the actuation signal. In addition, Fig. 9(b) shows that, when the study is run first without taking inertia into account, i.e. the static phase shown in Fig. 9(b), and then, when inertia is introduced, i.e. the dynamic phase shown in Fig. 9(b), such high frequency oscillations are not observed. This suggests that the initial high frequency oscillations seen with Fig. 9(a) may be caused by a sudden jump in the input signal. To verify this, further simulations were conducted using a step function as the driving signal. In particular, square waveforms of +/−140 V with different frequencies of 500 Hz and 100 Hz were applied to the simulated VAM set-up and are reported in Fig. 9(c) and (d). It can be observed from these two figures that indeed, a sudden change of input voltage causes high frequency oscillations of the workpiece, especially as a result of the actuation of the top piezoelectric plate. In addition, the dynamic response of the piezoelectric stack, but this time without the fixture and workpiece, was also simulated and the output displacements plotted with Fig. 9(e). Removing the fixture and the workpiece from this simulation run enabled to decrease the mass, and thus the inertial force, with a view to conduct a comparative analysis. When evaluated against Fig. 9(c), the simulated output of Fig. 9(e) shows an obvious reduction in high frequency vibrations. This indicates that for the current configuration of the VAM set-up developed, the mass of the fixture and of the workpiece has an effect. However, as discussed above, this effect should be present only for a very short time following the switching on of the driving signal and only for practical situations where this signal is such that it provides a sudden increase, or decrease, in the voltage delivered. Therefore, it could be said that the usage of sinusoidal driving waveforms should still lead to expected outcomes despite inertia.

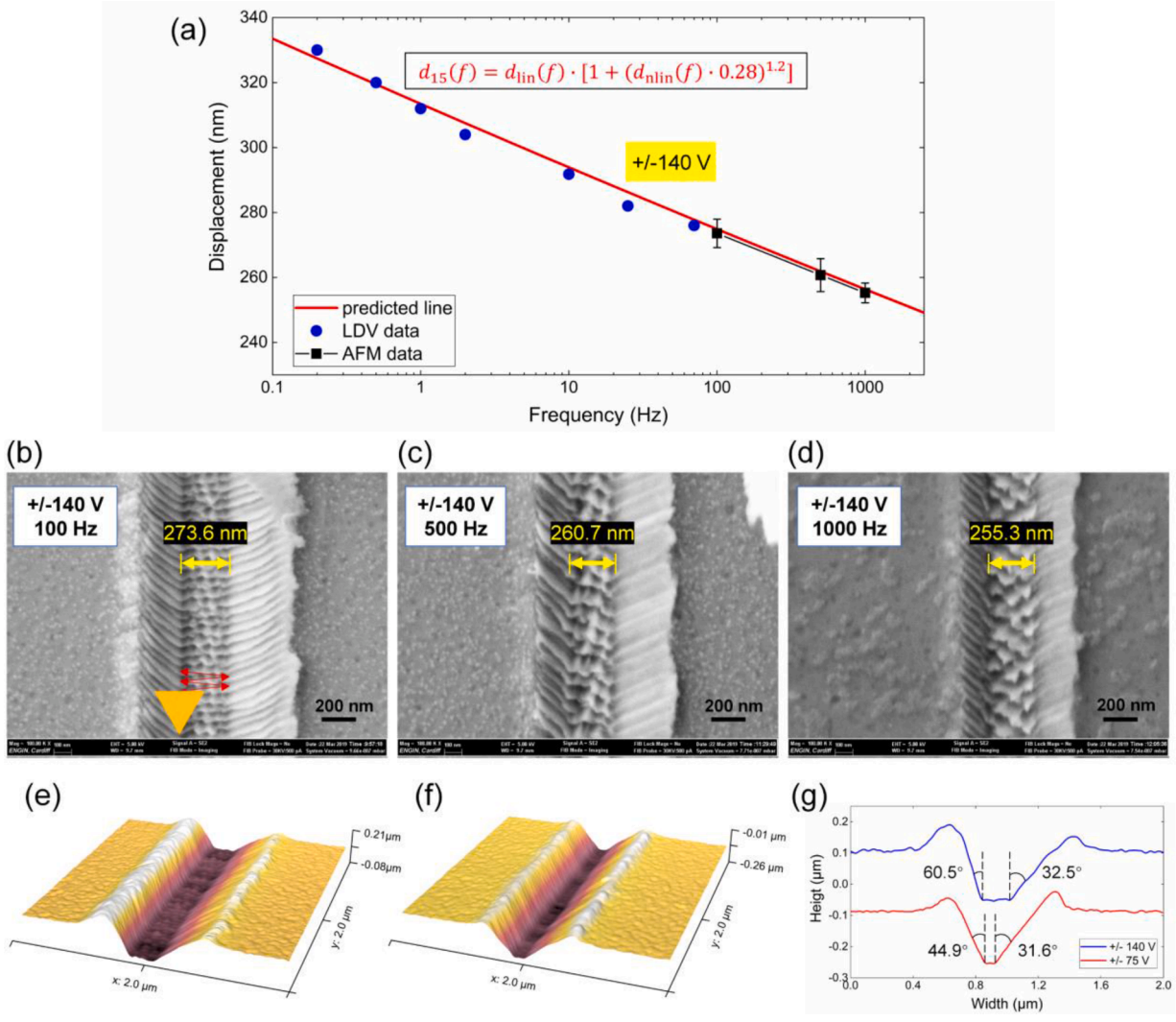

Fig. 10. (a) Comparison between experimental data (i.e. LDV measurements and measured widths at the bottom of grooves) and predicted frequency-dependant variations of displacement under the voltage of +/−140 V, (b)-(d) SEM images of machined nanogrooves and (e)-(g) AFM results of machined grooves.

3.3. Experimental validation of the proposed $d_{15}(E_1,f)$ function with nanoscale groove fabrication

Nanoscale groove fabrication experiments based on 1D in-plane VAM were conducted to validate the effectiveness of the designed piezoelectric actuation set-up for AFM-based VAM operations. Based on the FE model reported earlier in Fig. 2(b), the first resonant frequency of the AFM-based VAM set-up was calculated to be around 10,010 Hz under torsion mode and thus, far above the range of interest in this study (<3 kHz). In these experiments, three frequencies (100 Hz, 500 Hz and 1000 Hz) were also chosen to actuate the piezoelectric stack. However, a voltage of +/−140 V, not previously employed in the characterisation experiments, was also selected. Fig. 10(a) displays the comparison between the obtained experimental and simulated results. The predicted line in this figure was obtained from the frequency-dependant $d_{15}(E_1,f)$ expression under fixed field E_1. It can be seen that the difference between the experimental data and the predicted results is small. More specifically, an average difference of about 0.45% was observed between the predicted and machined groove widths with 3.2% being the maximum deviation measured. In addition, Fig. 10(a) shows that the change in mean value of the width at the bottom of the groove as a function of the frequency is aligned with that predicted with the FE model. SEM images of machined grooves are also provided with Fig. 10 (b)-(d) while Figs. 10(e) and (f) show their 3D topographies when machined under the conditions of +/−140 V (100 Hz) and +/−75 V (100 Hz).

Due to the interaction forces between the tip and workpiece, the induced torsional deflection of the cantilever may also impact the width of machined grooves. To minimize tip-sample interaction forces, it was proposed to employ a low stiffness cantilever to machine heat softened samples in [55]. However, it has been reported previously that the deformation of the cantilever should be minimal when using a diamond tip mounted on a cantilever with large torsional rigidity [56,57]. In addition, it can be observed from Fig. 10(a) that, the AFM data can be regarded as a continuation of the LDV data. This indicates that the machining process led to groove widths which matched the displacement of the piezoelectric plates. In addition, it can be seen from Fig. 10 (g) that the right sidewalls of grooves machined under different interaction forces have similar slope values. This also suggests that any difference in torsional deformation of the cantilever could be considered negligible. The slope difference observed in Fig. 10(g) on the left side of the groove could be attributed to the influence of material accumulation. From these analyses, it can be concluded that with the proposed model, the width of nanoscale grooves can be predicted effectively.

4. Conclusions

To predict the displacements of a shear-type piezoelectric actuator under high electric field and high frequency conditions, nonlinear piezoelectric constitutive equations were implemented in a coupled field FE model. The distinguishing characteristic of the research reported here lies in demonstrating how the field-dependant power equation from Mueller and Zhang could be combined with the logarithmic frequency-dependant approach proposed by Damjanovic to build the constitutive equations of the developed coupled field FE model. Through the fitting of experimental data, the piezoelectric coefficient d_{15} was characterised as a function of both the applied electric field and the driving frequency. Nanoscale grooves were also fabricated using 1D in-plane AFM-based VAM operations under an excitation voltage not employed when defining the constitutive equations of the coupled field FE model. By comparing the width of machined nanoscale grooves for a range of frequencies against predicted values, the effectiveness of the proposed method to characterise and model the nonlinearity of a shear-type piezoactuator was verified. In the context of AFM-based VAM operations, this is particularly important to ensure that nanoscale grooves can be produced in a deterministic manner.

The coupled field FE model of the shear-type piezoelectric stack was also employed to simulate the relative motion between an AFM tip and a processed workpiece in the context of AFM-based VAM operations. These simulations indicated that, in addition to the displacement amplitude, the variation of the d_{15} coefficient would also affect the shape of the piezoelectric movement trajectory. The simulations also revealed that cutting loads which are typical of AFM-based nanomachining should have a negligible influence on the displacements of such shear-type piezoelectric actuator set-ups.

CRediT authorship contribution statement

Bo Xue: Conceptualization, Methodology, Software, Validation, Formal analysis, Investigation, Writing – original draft, Data curation, Visualization. **Emmanuel Brousseau:** Conceptualization, Methodology, Validation, Formal analysis, Supervision, Project administration, Funding acquisition, Writing – review & editing. **Chris Bowen:** Conceptualization, Methodology, Writing – review & editing, Supervision, Funding acquisition.

Declaration of Competing Interest

The authors declare that they have no known competing financial interests or personal relationships that could have appeared to influence the work reported in this paper.

Data Availability

Data will be made available on request.

Acknowledgements

The reported research was funded by the Engineering and Physical Sciences Research Council (EPSRC) under the grant EP/M020703/1. The first author also gratefully acknowledges complementary support from the National Natural Science Foundation of China (52105434). All data created during this research are openly available from Cardiff University data archive at http://doi.org/10.17035/d.2022.0220305153

References

[1] Bruzzone AAG, Costa HL, Lonardo PM, Lucca DA. Advances in engineered surfaces for functional performance. CIRP Ann 2008;57(2):750–69.
[2] Kasani S, Curtin K, Wu N. A review of 2D and 3D plasmonic nanostructure array patterns: fabrication, light management and sensing applications. Nanophotonics 2019;8(12):2065–89.
[3] Rogers JA, Nuzzo RG. Recent progress in soft lithography. Mater Today 2005;8(2):50–6.
[4] Engstrom DS, Porter B, Pacios M, Bhaskaran H. Additive nanomanufacturing–a review. J Mater Res 2014;29(17):1792–816.
[5] Li L, Hong M, Schmidt M, Zhong M, Malshe A, Huis B, Kovalenko V. Laser nano-manufacturing–state of the art and challenges. CIRP Ann 2011;60(2):735–55.
[6] Fang FZ, Zhang XD, Gao W, Guo YB, Byrne G, Hansen HN. Nanomanufacturing—Perspective and applications. CIRP Ann 2017;66(2):683–705.
[7] Zhang J, Cui T, Ge C, Sui Y, Yang H. Review of micro/nano machining by utilizing elliptical vibration cutting. Int J Mach Tools Manuf 2016;106:109–26.
[8] Xu S, Kuriyagawa T, Shimada K, Mizutani M. Recent advances in ultrasonic-assisted machining for the fabrication of micro/nano-textured surfaces. Front Mechan Eng 2017;12(1):33–45.
[9] Yang Z, Zhu L, Zhang G, Ni C, Lin B. Review of ultrasonic vibration-assisted machining in advanced materials. Int J Mach Tools Manuf 2020;156:103594.
[10] Yan Y, Geng Y, Hu Z. Recent advances in AFM tip-based nanomechanical machining. Int J Mach Tools Manuf 2015;99:1–18.
[11] Park SS, Mostofa MG, Park CI, Mehrpouya M, Kim S. Vibration assisted nano mechanical machining using AFM probe. CIRP Annals - Manuf Technol 2014;63(1):537–40.
[12] Zhang L, Dong JY, Cohen PH. Material-insensitive feature depth control and machining force reduction by ultrasonic vibration in AFM-based nanomachining. IEEE Trans Nanotechnol 2013;12(5):743–50.

[13] Geng Y, Yan YD, Zhuang Y, Hu ZJ. Effects of AFM tip-based direct and vibration assisted scratching methods on nanogrooves fabrication on a polymer resist. Appl Surf Sci 2015;356:348–54.
[14] Brehl DE, Dow TA. Review of vibration-assisted machining. Precis Eng 2008;32:153–72.
[15] Zhang L, Dong JY. High-rate tunable ultrasonic force regulated nanomachining lithography with an atomic force microscope. Nanotechnology 2012;23(8):085303.
[16] Gozen BA, Ozdoganlar OB. Design and evaluation of a mechanical nanomanufacturing system for nanomilling. Precision Eng 2012;36(1):19–30.
[17] Geng Y, Brousseau EB, Zhao X, Gensheimer M, Bowen CR. AFM tip-based nanomachining with increased cutting speed at the tool-workpiece interface. Precis Eng 2018;51:536–44.
[18] Hassani V, Tjahjowidodo T, Do TN. A survey on hysteresis modeling, identification and control. Mechan syst signal process 2014;49(1–2):209–33.
[19] Sabarianand DV, Karthikeyan P, Muthuramalingam T. A review on control strategies for compensation of hysteresis and creep on piezoelectric actuators based micro systems. Mech Syst Signal Process 2020;140:106634.
[20] Geng Y, Li H, Yan Y, He Y, Zhao X. Study on material removal for nanochannels fabrication using atomic force microscopy tip-based nanomilling approach, Proceedings of the Institution of Mechanical Engineers, Part B. J Eng Manuf 2019;233(2):461–9.
[21] Yan Y, Xue B, Hu Z, Wu D. Machining slight burr formed micro-channels with different moving trajectories of a pyramidal diamond tip. The Int J Adv Manuf Technol 2016;84(9):2037–46.
[22] Sezer N, Koc M. A comprehensive review on the state-of-the-art of piezoelectric energy harvesting. Nano Energy 2021;80:105567.
[23] Sharma S, Kiran R, Azad P, Vaish R. A review of piezoelectric energy harvesting tiles: available designs and future perspective. Energy Convers Manage 2022;254:115272.
[24] Wang S, Rong W, Wang L, Xie H, Sun L, Mills JK. A survey of piezoelectric actuators with long working stroke in recent years: classifications, principles, connections and distinctions. Mech Syst Signal Process 2019;123:591–605.
[25] Gao X, Yang J, Wu J, Xin X, Li Z, Yuan X, Shen X, Dong S. Piezoelectric actuators and motors: materials, designs, and applications. Adv Mater Technol 2020;5(1):1900716.
[26] Reddy RS, Panda S, Gupta A. Nonlinear dynamics and active control of smart beams using shear/extensional mode piezoelectric actuators. Int J Mech Sci 2021;204:106495.
[27] Gao X, Xin X, Wu J, Chu Z, Dong S. A multilayered-cylindrical piezoelectric shear actuator operating in shear (d15) mode. Appl Phys Lett 2018;112(15):152902.
[28] Gozen BA, Ozdoganlar OB. A rotating-tip-based mechanical nano-manufacturing process: nanomilling. Nanoscale Res Lett 2010;5(9):1403–7.
[29] Wang J, Yan Y, Geng Y, Gan Y, Fang Z. Fabrication of polydimethylsiloxane nanofluidic chips under AFM tip-based nanomilling process. Nanoscale Res Lett 2019;14(1):1–14.
[30] Wang J, Yan Y, Li Z, Geng Y. Towards understanding the machining mechanism of the atomic force microscopy tip-based nanomilling process. Int J Mach Tools Manuf 2021;162:103701.
[31] Upadrashta D, Yang Y. Finite element modeling of nonlinear piezoelectric energy harvesters with magnetic interaction. Smart Mater Struct 2015;24(4):045042. 13 pp.
[32] Kuang Y, Zhu M. Evaluation and validation of equivalent properties of macro fibre composites for piezoelectric transducer modelling. Composites Part B: Eng 2019;158:189–97.
[33] Zhang Q, Chen W, Liu Y, Liu J, Jiang Q. A frog-shaped linear piezoelectric actuator using first-order longitudinal vibration mode. IEEE Trans Ind Electron 2016;64(3):2188–95.
[34] Kranz B, Benjeddou A, Drossel WG. Numerical and experimental characterizations of longitudinally polarized piezoelectric d_{15} shear macro-fiber composites. Acta Mech 2013;224(11):2471–87.
[35] Wang DW, Mo JL, Wang XF, Ouyang H, Zhou ZR. Experimental and numerical investigations of the piezoelectric energy harvesting via friction-induced vibration. Energy Convers Manage 2018;171:1134–49.
[36] Li S, Cao W, Cross L. The extrinsic nature of nonlinear behavior observed in lead zirconate titanate ferroelectric ceramic. J Appl Phys 1991;69(10):7219–24.
[37] Perez R, Albareda A, Garcia JE, Tiana J, Ringgaard E, Wolny WW. Extrinsic contribution to the non-linearity in a PZT disc. J Phys D Appl Phys 2004;37(19):2648.
[38] Garcia JE, Perez R, Ochoa DA, Albareda A, Lente MH, Eiras JA. Evaluation of domain wall motion in lead zirconate titanate ceramics by nonlinear response measurements. J Appl Phys 2008;103(5):054108.
[39] Tutuncu G, Forrester JS, Chen J, Jones JL. Extrinsic contributions to piezoelectric Rayleigh behavior in morphotropic PbTiO3-BiScO3. Acta Mater 2017;137:45–53.
[40] Mueller V, Zhang Q. Shear response of lead zirconate titanate piezoceramics. J Appl Phys 1998;83(7):3754–61.
[41] Benjeddou A. Field-dependent nonlinear piezoelectricity: a focused review. Int J Smart and Nano Mater 2018;9(1):68–84.
[42] Bowen C, Kim H, Weaver P, Dunn S. Piezoelectric and ferroelectric materials and structures for energy harvesting applications. Energy Environ Sci 2014;7(1):25–44.
[43] Thornburgh RP, Chattopadhyay A. Nonlinear actuation of smart composites using a coupled piezoelectric-mechanical model. Smart Mater Struct 2001;10(4):743.
[44] Trindade MA, Benjeddou A. Finite element characterization and parametric analysis of the nonlinear behaviour of an actual d15 shear MFC. Acta Mech 2013;224(11):2489–503.
[45] Trindade MA, Benjeddou A. Finite element characterisation of multilayer d31 piezoelectric macro-fibre composites. Compos Struct 2016;151:47–57.
[46] Trindade MA, Benjeddou A. Finite element characterization and parametric analysis of the nonlinear behaviour of an actual d_{15} shear MFC. Acta Mech 2013;224:2489–503.
[47] Malakooti MH, Sodano HA. Direct measurement of piezoelectric shear coefficient. J Appl Phys 2013;113:214106. 6 pp.
[48] Masys AJ, Ren W, Yang G, Mukherjee BK. Piezoelectric strain in lead zirconate titante ceramics as a function of electric field, frequency, and dc bias. J Appl Phys 2003;94(2):1155–62.
[49] Damjanovic D. Logarithmic frequency dependence of the piezoelectric effect due to pinning of ferroelectric-ferroelastic domain walls. Phys Rev B 1997;55(2):R649–52.
[50] Fialka J, Benes P. Comparison of methods of piezoelectric coefficient measurement. In: 2012 IEEE International Instrumentation and Measurement Technology Conference Proceedings; 2012. p. 37–42.
[51] Hall DA. Review nonlinearity in piezoelectric ceramics. J Mater Sci 2001;36(19):4575–601.
[52] Moheimani SR, Fleming AJ. Piezoelectric transducers for vibration control and damping, 1. London: Springer; 2006. VolChapter 11.
[53] Islam S, Ibrahim R, Das R, Fagan T. Novel approach for modelling of nanomachining using a mesh-less method. Appl Math Model 2012;36(11):5589–602.
[54] Kong X, Dong J, Cohen PH. Modeling of the dynamic machining force of vibration-assisted nanomachining process. J Manuf Process 2017;28:101–8.
[55] Zhou H, Dmuchowski C, Ke C, Deng J. External-energy-assisted nanomachining with low-stiffness atomic force microscopy probes. Manuf Lett 2020;23:1–4.
[56] Yan YD, Dong S, Sun T. 3D force components measurement in AFM scratching tests. Ultramicroscopy 2005;105(1–4):62–71.
[57] Geng Y, Yan Y, Xing Y, Zhang Q, Zhao X, Hu Z. Effect of cantilever deformation and tip-sample contact area on AFM nanoscratching. J Vacuum Sci Technol B 2013;31(6):061802.